11th World Congress on Computational Mechanics (WCCM XI)
5th European Conference on Computational Mechanics (ECCM V)
6th European Conference on Computational Fluid Dynamics (ECFD VI)
E. Oñate, J. Oliver and A. Huerta (Eds)

AERODYNAMICS AND AEROACOUSTICS STUDY OF THE FLOW AROUND AN AUTOMOTIVE FAN AIRFOIL

RABEA MATOUK*, GERARD DEGREZ† AND JULIEN CHRISTOPHE‡

* Université Libre de Bruxelles
Rue Emile Banning 124, B-1050 Brussels, Belgium
e-mail: rabea.matouk@ulb.ac.be

† Université Libre de Bruxelles
CP 165/43, 50 Av. F.D. Roosevelt, B-1050 Brussels, Belgium
e-mail: gdegrez@ulb.ac.be

‡ von Karman Institute for Fluid Dynamics
72 Chausée de Waterloo, B-1640 Rhode-st-genèse, Belgium
e-mail: julien.christophe@vki.ac.be

Key words: LES, CD (Controlled-Diffusion) Airfoil, Pressure spectrum, Smagorinsky, WALE, Amiet.

Abstract. This paper presents the results of aerodynamic simulations of the flow around a CD (Controlled-Diffusion) airfoil for the turbulent regime by the in-house SFELES solver which is a hybrid spectral/finite elements code capable of simulating 3D unsteady incompressible viscous flows over axisymmetric and planar geometries with a direction of periodicity. The results are compared with experimental results obtained by Moreau and Roger [1] and Moreau et al. [2] as well as other numerical results performed by J.Christophe [4] using OpenFoam. The simulations were carried out for Re=160,000 in order to study the unsteady turbulent boundary layer and to calculate the wall pressure spectrum used for noise predictions. Several SGS models, such as the static Smagorinsky model, the WALE model and the model proposed by G.Ghorbaniasl [5], were used and their results were compared to study the influence of the LES sub grid-scale on the results. Amiet's aeroacoustic theory [6, 7] is then applied using the wall pressure spectrum for a station near the trailing edge in order to calculate the trailing-edge noise. The sound pressure level and its directivity are computed for the three SGS models and compared with experiments.

1 INTRODUCTION

Several experimental and numerical studies (finite volumes and finite differences simulations) were performed on the CD airfoil in order to study the unsteady and turbulent

boundary layer and wake in order to calculate the noise sources for sound predictions. The broadband self-noise generated by this particular airfoil is mainly due to the trailing-edge noise produced by the scattering of the boundary layer at trailing edge. The reader is referred to [4] where most of studies are reported. The first LES numerical study has been performed by Wang [9], by LES hybrid finite differences/spectral code. Another recent study has been performed by Christophe [4], by a LES Fluent and OpenFoam finite volumes simulations. The two studies have been achieved on a sub-domain around the airfoil using velocities, extracted from a RANS simulation performed by Wang [9] on a larger domain including the jet and the airfoil, as boundary conditions on the LES domain inlet. It has bean shown by Moreau [3] that there are significant differences between the results obtained from a simulation performed on an isolated airfoil in a uniform stream and that performed on an airfoil in an open-jet wind tunnel facility. The same procedure is applied in our study and the velocities, extracted from the RANS simulation are used as inlet boundary condition. In the present work SFELES is used to solve the flow.
SFELES [10] is a hybrid spectral/finite elements code capable of simulating 3D unsteady incompressible viscous flows over axisymmetric and planar geometries. It is large eddy simulation solver based on a combination of a spectral discretization in the periodic (azimuthal or transverse) direction and a finite elements discretization in the perpendicular (meridian or longitudinal) plane. The main advantage of this code is its ability to exploit the existence of a direction of periodicity in the geometry to increase the computational efficiency.
Three SGS models have been used in the present study. The first is the Smagorinsky model [11] with $C_s = 0.17$. The second model considered is the WALE model [12] with $C_w = 0.55$. The third model is a recent model proposed by Ghorbaniasl [5]. In this model the Smagorinsky constant C_s is supposed to be a function of the flow variables including the rotational and translational velocities. The final formulation of this model is:

$$C_s = min(G_x, G_y, G_z) \tag{1}$$

where $G_x = \frac{|\bar{\Omega}_x \bar{u}_x|}{2D}$, $G_y = \frac{|\bar{\Omega}_y \bar{u}_y|}{2D}$, $G_z = \frac{|\bar{\Omega}_z \bar{u}_z|}{2D}$ and $D = \sqrt{(\bar{\Omega}_x \bar{u}_x)^2 + (\bar{\Omega}_y \bar{u}_y)^2 + (\bar{\Omega}_z \bar{u}_z)^2}$. The constant C_s is computed dynamically but without the need of dynamic procedure which means a gain of time computation. This model has been validated for simple cases (channel flow and circular cylinder) and for low Reynolds numbers (180 and 3900) by Ghorbaniasl [5]. In this work, it is implemented in SFELES and tested for a more complicated case (the CD airfoil) for high Reynolds number (160000). SFELES uses the stabilized Galerkin FEM method where the added stabilizations terms are the SUPG (Streamline - Upwind Petrov - Galerkin) and the PSPG (Pressure Stabilised Petrov - Galerkin) [13, 14]. It is assumed that the flow in the spanwise direction is periodic and known at discrete points in space, therefore the pressure and velocity can be developed as a sum of discrete Fourier modes [10, 16]. Considering the temporal discretization, Crank-Nicolson method is used for the pressure and diffusive terms while Adams-Bashforth method is used for convective terms.

2 CASE DEFINITION

Fig. 1 shows the automotive cooling module, its 9-blades rotor and the profile of the blade, cut at mid-span, on which all simulations were performed. It is located in the middle of the blade span. The airfoil thickness is $4\%C$ and Its camber angle is 12°. The chord length is $C = 0.1356$ m. The airfoil is set at 8° angle of attack. The spanwise dimension of the numerical domain is 10% of the chord length. Fig. 2 shows the computational

Figure 1: The automotive cooling module, its 9-blades fan and the airfoil of the blade

domain with the used mesh. The size of the computational domain is 4C in the streamwise direction (x) and 2.5C in the transverse direction (y). The domain was divided into triangular elements with nearly 160,000 elements and nearly 80,000 nodes. This mesh is refined to capture small perturbations in the flow. The refinement was done such that the first grid points of the surface lie within 1.1 wall units of the wall ($y^+ < 1.1$). Velocity was

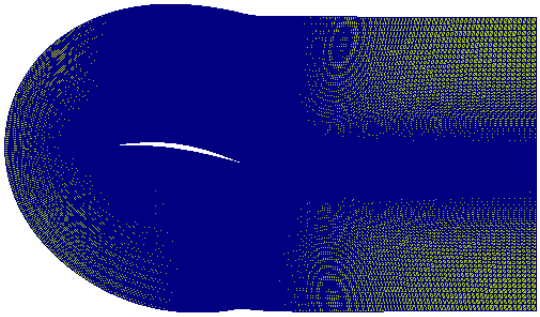

Figure 2: The computational domain with the structured mesh

prescribed on the inlet (along the outer C boundary), pressure was imposed on the outlet (it is imposed equal to 0) and no-slip conditions were imposed on the airfoil. Inlet velocity profiles on the restricted domain were extracted from RANS computations. Furthermore, a periodicity condition in the spanwise direction (z) was assumed. In order to trigger 3D instabilities, some random perturbations (noise) are added to the solution during the simulation for a period of 0.4 time units t*, where $t^* = \frac{t*U_0}{C}$, for all mesh nodes. This is a good way to start the turbulent motions where the intensity of the fluctuations applied is 0.1% for all turbulent simulations.

3 RESULTS AND DISCUSSION OF THE AERODYNAMIC SIMULATIONS

Five simulations of the CD-profile were performed by changing the Reynolds number and the number of spanwise Fourier modes according to the table 1:

Table 1: The simulations performed on the profile

Simulation	Re	Fourier modes	Regime type	Time step (sec)	Time t*	SGS model
1	$1.6*10^5$	32 (3d)	Turbulent	$\Delta t = 5.10^{-6}$	12	Smagorinsky
2	$1.6*10^5$	64 (3d)	Turbulent	$\Delta t = 5.10^{-6}$	12	Smagorinsky
3	$1.6*10^5$	64 (3d)	Turbulent	$\triangle t = 1.10^{-6}$	12	WALE
4	$1.6*10^5$	32 (3d)	Turbulent	$\triangle t = 1.10^{-6}$	12	Ghorbaniasl
5	$1.6*10^5$	64 (3d)	Turbulent	$\triangle t = 5.10^{-6}$	12	Ghorbaniasl

3.1 Flow topology

Figure 3 shows the flow topology described by the contour of the Q criterion with $Q = \frac{1}{4}(\omega^2 + 2S_{ij}S_{ij})$. The figure depicts the level of vorticity and the size of turbulent structures in the flow at a given instant for all simulations. The turbulent flow around the profile can be characterized by a laminar boundary layer on the lower surface and a turbulent and transient boundary layer on the upper surface. It is also noticed that there is a recirculation bubble near the leading edge. It is found that the bubble size highly depends on the solver and the SGS model as shown in table 2. In this table, the recirculation bubble size is compared for the present simulations and for most simulations already performed on the CD airfoil including several solvers, numerical methods and SGS models. It is clear that LES with the static Smagorinsky model overpredicts the bubble size regardless the numerical method used in the solver whereas with the dynamic Smagorinsky and Ghorbaniasl, its size is more reasonable. RANS predicts well the recirculation bubble whereas DES can not reproduce it. Moreover, the vorticity is more intense for 64 Fourier

Table 2: Recirculation bubble size: comparsion with other simulations

Author	Method/Solver	SGS model	Bubble size
Matouk (This study)	LES FEM spectral/SFELES	Static Smagorinsky 64M	8.4%C
		Static Smagorinsky 32M	9.8%C
		Ghorbaniasl 64M	3.5%C
		Ghorbaniasl 32M	3.55%C
		WALE 64M	7%C
Christophe [4]	LES FV/OpenFoam	Dynamic Smagorinsky	5.26%C
	LES FV/Fluent	Dynamic Smagorinsky	5.04%C
Wang [9]	LES FD/spectral (Re=150000)	Dynamic Smagorinsky	3.7%C
	RANS	SST $k-\omega$	3.1%C
Moreau [15]	LES FVM/STAR-CD (Re=120000)	Static Smagorinsky	11.2%C
	DES FVM/STAR-CD (Re=120000)	$k-\varepsilon$	0

modes than for 32 modes and there are many more structures in this case, because more information is resolved about the flow. The figure shows that the nature of the developed turbulent structures is largely influenced by the size and the structure of the recirculation bubble. In the simulation with Ghorbaniasl's model, the turbulent structures are finer and

more intense than for the simulation with the Smagorinsky model but the total energy convected at the trailing edge is almost the same as it will be shown when the wall-pressure spectrum is computed (see Fig. 6). Furthermore, a small vortex shedding from the pressure side is noticed. It is more important for with Ghorbaniasl's model, especially for 64M. This shedding depends largely on the angle of attack of the profile and the free stream velocity [8]. It has important effects when the calculation of the total noise is requested. A narrow-band or tonal contribution is added to the overall sound [8].

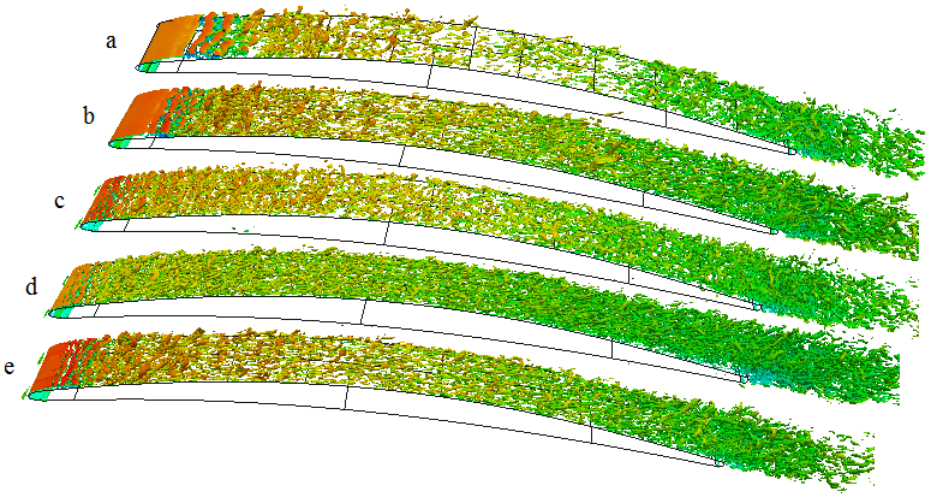

Figure 3: Topology of the flow for all simulations described by the criterion Q($Q.\frac{C^2}{U_0^2} = 1000$) and colored by the longitudinal instantaneous velocity with the model: a) Smagorinsky 32M, b) Smagorinsky 64M, c) Ghorbaniasl 32M, d) Ghorbaniasl 64M, e) WALE 64M

3.2 Pressure and friction coefficients distribution on the airfoil surface

Figure 4 shows the mean pressure and friction coefficients distribution on the airfoil. As far as the pressure distribution is concerned, first considering the Smagorinsky and WALE results, one observes a very good agreement with experimental results as well as OpenFoam simulations except near the leading edge where the results are influenced by the size of the recirculation bubble which is larger than in OpenFoam results as mentioned above. In contrast, for Ghorbaniasl's model, we have a very good agreement with OpenFoam's results in this region. As far as skin friction on the upper surface is concerned, there is a region toward the leading edge in which the friction coefficient is negative, this region corresponds to the recirculation bubble. Downstream of the reattachment, the present results are seen to be in good agreement with the OpenFoam results in particular, for the simulation with 64 M using Ghorbaniasl's model. The skin friction on the lower surface is uniform and less important because the boundary layer is laminar.

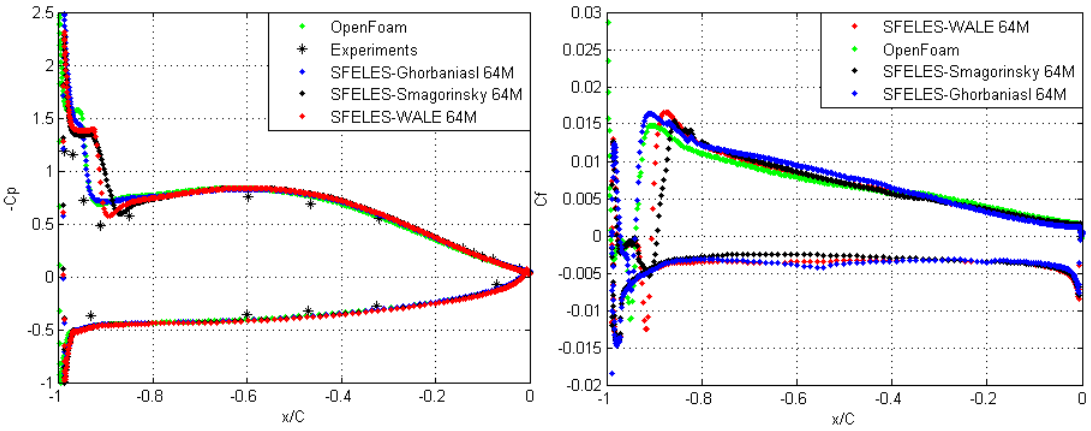

Figure 4: (left) Average pressure coefficient (Cp) distribution and (right) Skin Friction coefficient (Cf) distribution

3.3 Boundary layer velocity profiles

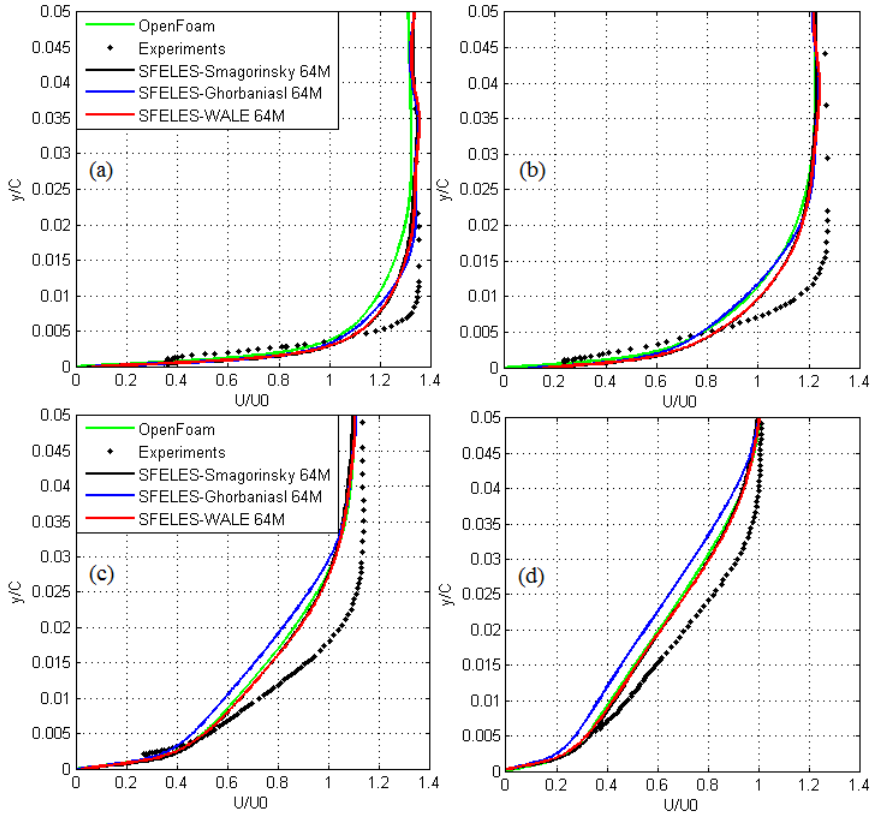

Figure 5: Average velocity profiles in the boundary layer on the upper surface in several sections a) x/C = -0.6, b) x/C = -0.32, c) x/C = -0.14, d) x/C = -0.02

The average longitudinal velocity profiles in the boundary layer have been extracted in several positions along the airfoil ($x/C = -0.6$, $x/C = -0.32$, $x/C = -0.14$ and $x/C = -0.02$) as illustrated in Fig. 5. In our mesh the trailing edge corresponds to($x/C = 0$) and the leading edge corresponds to($x/C = -1$), x is aligned with the chord and pointing in the streamwise direction, y is crosswise. It is noticed that the thickness of the boundary layer developed on the upper surface increases from the leading edge to the trailing edge. One observes on Fig. 5 a very good agreement with the OpenFoam simulations as well as with the experimental results when the boundary layer thickness is considered and as a general profiles. Average quantity were obtained by averaging in spanwise direction and in time for 7t*.

3.4 Wall pressure spectra

The pressure evolution with respect to time was acquired and averaged spanwise in two positions near the trailing edge on the suction side: x/C=-0.08 and x/C=-0.02 during a period of 6t* for all simulations. Then, wall-pressure spectra are computed and compared with OpenFoam and the experimental results. The pressure spectra are expressed as the Power Spectral Density (PSD). In order to express the PSD in [dB], the following transformation is applied: $SPL = 20log_{10}(\frac{\sqrt{G_{pp}(f)}}{P_0})$ Where $P_0 = 2 * 10^{-5}[pa]$ is the reference pressure. Welch method is used in order to estimate the spectra with applying the averaging over segments of 2^9 points and with a multiplication by a Hanning window and overlap 50% between the segments. The results are illustrated in Fig. 6 . At the two positions, the

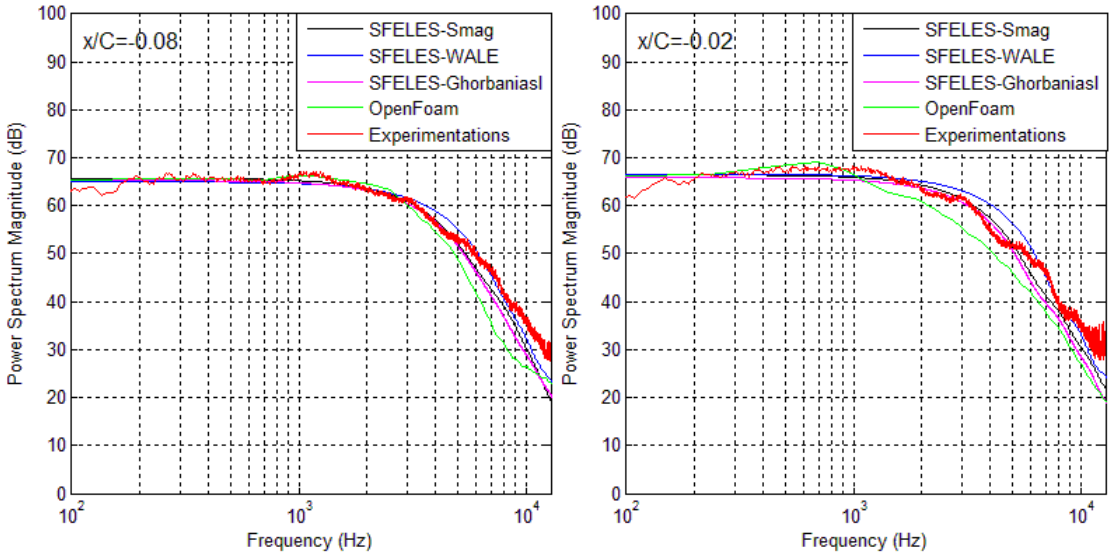

Figure 6: Power Spectral Density of pressure fluctuations at the positions: x/C=-0.08, x/C=-0.02 (comparison with OpenFoam and the experiments)

results show a very good agreement with the experiments and OpenFoam especially for

the low and mid frequency ranges for the three SGS models with a difference up to 2dB. At high frequencies, SFELES results are closer to experiments than OpenFoam. There are little differences between the SGS models, WALE and Smagorinsky curves are closer to the experiments. In contrast, the Ghorbaniasl's model curve is dropping quicker. It is noticed that the recirculation bubble size does not influence the pressure spectra for the sections near the trailing edge so it will have little effects on the radiated sound.

4 AEROACOUSTIC STUDY: THE APPLICATION OF AMIET'S THEORY

Broadband self-noise or trailing edge noise, caused by the scattering of the blade turbulent boundary layer at the trailing edge into acoustic waves, is a major contributor of the overall radiated noise. It is the minimum noise that could be produced by the rotating machines [19]. In this paper, Amiet's theory with its extensions [6, 7] is applied in order to calculate this noise in the far field using LES input data represented by the wall pressure spectrum already calculated in a point near the trailing edge ($x/C = -0.02$). This procedure is physically justified by the fact that when the incident aerodynamic wall pressure is convected past the trailing edge, it behaves as equivalent acoustic sources. Amiet's model describes how the hydrodynamic waves convected within the boundary layer are scattered by the trailing edge; thereby unsteady loads are generated over the blade surface. The noise is generated by these forces. Schwarzschild's procedure [17] is applied iteratively such that the turbulent boundary layer is considered as a series of waves traveling towards the trailing edge. Each scattered wave gives rise to an upstream traveling wave such that the total pressure vanishes downstream the flat plate. These scattered waves create the unsteady loads which generate the noise. It is assumed that the airfoil is a flat plate (the thickness of the blade isn't considered in the model directly but within the pressure spectrum) extended to the infinity in the downstream direction so it is restricted to high frequencies. The extension to include low frequencies was developed by Roger & Moreau [7] by taking into account the back-scattering from the leading edge, accounting for the finite chord length, in the model. This is done using a two-step Schwarzschild's solution [7]. The final far-field acoustic pressure power spectral density formula applied in this paper for a given frequency ω is:

$$S_{pp}(X,\omega) = (\frac{sin\theta}{2\pi R})^2.(kC)^2 d.|\Gamma|^2 \Phi_{pp}(\omega) l_y(\omega) \tag{2}$$

The reader is referred to [7] for the complete derivation. In this equation d is the mock-up semi-span, where the span is assumed to equal to $40C$, C is the airfoil chord length, k is the acoustic wavenumber. $R = 2$ m and $\theta = 90^o$ are the listener location which is placed in the mid-span plane above the trailing edge in our case. $\Phi_{pp}(\omega)$ is the wall-pressure power spectral density and $l_y(\omega)$ is the spanwise correlation length near the trailing edge which is computed using the Corcos's model [18] given by the relation: $l_y(\omega) = \frac{b.U_c}{\omega}$ with $U_c = 0.7U_0$ the convection speed and the coefficient $b = 1.5$. Γ is the aeroacoustic transfer

function ($\Gamma = \Gamma_1 + \Gamma_2$) with Γ_1 is the transfer function of the trailing edge and Γ_2 is the back-scattering leading edge correction.

4.1 Results and discusion

Fig. 7 shows the PSD of the sound pressure level at the considered observer. First, considering the left Figure without the leading edge back-scattering correction, we have a very good agreement with the experimental results with a discrepancies up to 2 dB at low frequencies,it is expected because the actual chord length is not yet considered. Second, on the right Figure where the leading edge correction is applied, the results are improved for low frequencies between 100 and 300 Hz as expected. The back-scattering correction has no important influences on the results for high frequencies. It is clear that SFELES results are in very good agreement with experimental results and closer than OpenFoam in particular for frequencies between 1500 and 2000 Hz. Comparing with OpenFoam results, the results are in good agreement in the domain 100-1500 Hz and then our curves have higher values but closer to experimental results (1500-2000 Hz), this is linked directly to the the differences in the wall pressure spectra estimation, (see Fig. 6). As far as the comparison between the three used SGS models is concerned, one can notice that there are no important differences because the wall-pressure spectra were very similar, the difference does not exceed 2 dB in the domain of interest (100-2000 Hz). The directivity patterns of the acoustic pressure are shown in Fig. 8 for the three SGS models. The behavior is very similar in the three cases. The dipolar behavior is clear where there are two big dominant lobes, they multiply and orient towards the leading edge for high frequencies. The secondary lobes are more important when the WALE model is considered at the frequency 1804 Hz

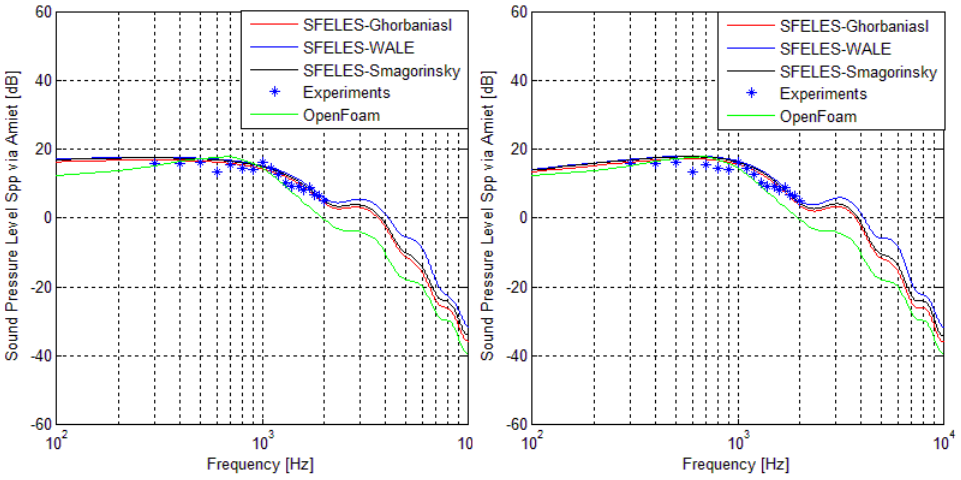

Figure 7: Trailing edge sound using Amiet's theory for the three SGS models (left) without the leading edge correction (right) with the leading edge correction, comparison with OpenFoam and Experiments. The receiver is placed in the mid-span plane above the trailing edge (R=2 m, $\theta = 90^o$)

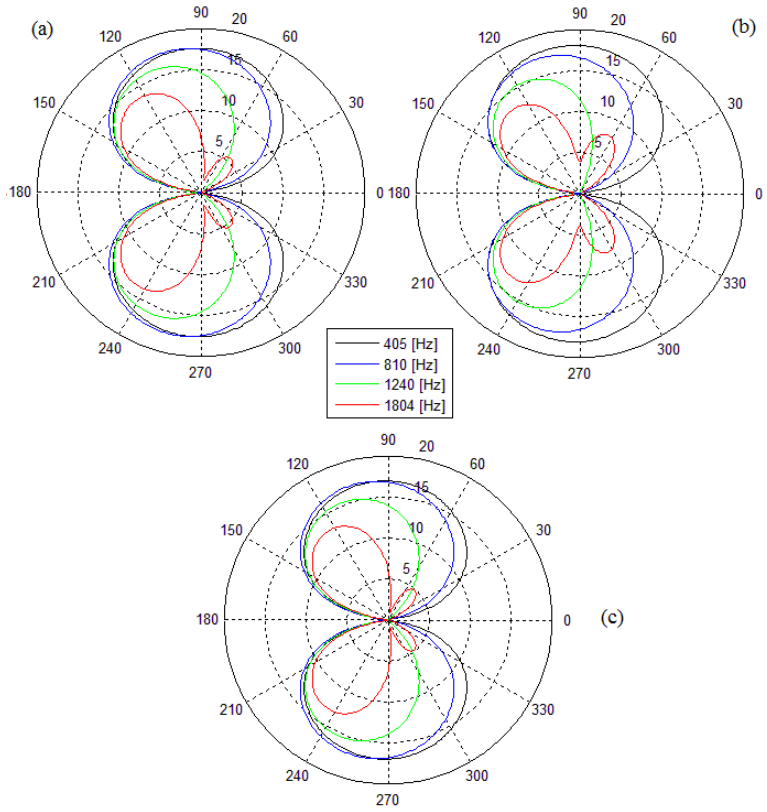

Figure 8: The noise directivity patterns [dB] for all SGS model, (a): Smagorinsky, (b): WALE, (c): Ghorbaniasl

5 CONCLUSION

In the present paper, aerodynamics and aeroacoustics study of the CD Valeo profile is performed. The in-house solver SFELES is used to solve the flow. Average pressure and friction coefficients distribution, boundary layer profiles and the wall-pressure spectra are computed and compared with experimental and OpenFoam results. Three turbulence models are used which are the static Smagorinsky model, the WALE model and Ghorbaniasl's model. Amiet's aeroacoustics theory is then applied using the wall-pressure spectrum extracted near the trailing edge during the simulations as input data. The sound pressure level and its directivity are computed for the three SGS models and compared. The main observations were made are:

- First considering the aerodynamics results:
  - A good agreement is obtained in general with previous experimental and numerical studies with differences in the region towards the leading edge due to the high variability of the leading edge recirculation bubble size with the solver and the SGS model as shown in table 2.

  - The new SGS model proposed by G.Ghorbaniasl is implemented and validated. It is found that the results are improved in general, especially near the leading edge, comparing with OpenFoam and experimental results. The recirculation bubble size is found equal to 3.5%C.
  - The recirculation bubble size has no important effects on the wall-pressure spectra near the trailing edge whereas it influences largely the pressure and friction coefficients in the region near the leading edge.
  - The wall-pressure spectrum computed by SFELES is in excellent agreement with experiments and better than OpenFoam for frequencies between 1000 Hz and 5000 Hz.

- Second considering the aeroacousitcs results: The predicted noise obtained using the wall-pressure spectrum of SFELES are in very good agreement with experimental results and closer than OpenFoam in particular for frequencies between 1000 and 2000 Hz regardless of the SGS model. The dipolar behaviour of the noise sources is found and the lobes multiply and orient towards the leading edge for high frequencies when the acoustic pressure directivity is considered. The secondary lobes are more important when the WALE model is considered at the frequency 1804 Hz.

References

[1] S. Moreau and M. Roger. *Effect of Airfoil Aerodynamic Loading on Trailing-Edge Noise Sources*. AIAA Journal, 43(1):41–52, January 2005.

[2] S. Moreau, D. Neal, and J. Foss. *Hot-Wire Measurements Around a Controlled Diffusion Airfoil in an Open-Jet Anechoic Wind Tunnel*. J. Fluids Eng, 128:699-706, 2006.

[3] S.Moreau , G.Iaccarino, M.Roger AND M.Wang. *CFD analysis of flow in an open-jet aeroacoustic experiment*. Center for Turbulence Research Annual Research Briefs, 343-351, 2001.

[4] J. Christophe. *Application of Hybrid Methods to High Frequency Aeroacoustics*. PhD Thesis, Université Libre de Bruxelles, 2011.

[5] G. Ghorbaniasl,V. Agnihotri,C. Lacor. *A self-adjusting flow dependent formulation for the classical Smagorinsky model coefficient*. Physics of Fluids, 25, 099101, 2013.

[6] R. K. Amiet. *Noise due to Turbulent Flow past a Trailing Edge*. Journal of Sound and Vibration, 47(3):387-393, 1976.

[7] M. Roger and S. Moreau. *Back-Scattering Correction and Further Extensions of Amiet's Trailing-Edge Noise Model. Part 1: Theory* . Journal of Sound and Vibration, 286:477-506, 2005.

[8] S. Moreau and M. Roger. *Back-Scattering Correction and Further Extensions of Amiet's Trailing-Edge Noise Model. Part 2: Application* . Journal of Sound and Vibration, 323:397-425, 2009.

[9] M. Wang, S. Moreau, G. Iaccarino, and M. Roger. *LES Prediction of Pressure Fluctuations on a Low Speed Airfoil*. In Annual Research Briefs. Centre for Turbulence Research, Stanford Univ./NASA Ames, 2004.

[10] D.Snyder. *A parallel finite-element/spectral LES algorithm for complex two dimensional geometries*. PhD Thesis, von Karman Institute for Fluid Dynamics, Belgium, Utah State University, USA 2002.

[11] J.Smagorinsky. *General circulation experiments with the primitive equations part I: the basic experiment*. Monthly Weather Review, 91:99−164, 1963.

[12] Nicoud F, Ducros F. *Subgrid-Scale Stress Modelling Based on the Square of the Velocity Gradient Tensor*. Flow, Turbulence and Combustion, 1999.

[13] T.E. Tezduyar, S. Mittal, S.E. Ray, and R. Shih. *Incompressible flow computations with stabilized bilinear and linear equal-order interpolation velocity- pressure elements*. Comput. Methods Appl. Mech. Engrg, 95:221−242, 1992.

[14] T.E. Tezduyar and Y. Osawa. *Finite element stabilization parameters computed from element matrices and vectors*. Comput. Methods Appl. Mech. Engrg, 190:411−430, 2000.

[15] S. Moreau, F. Mendonca, O. Qazi, R. Prosser, and D. Laurence. *Influence of Turbulence Modeling on Airfoil Unsteady Simulations of Broadband Noise Sources*. In 11thAIAA/ CEAS Aeroacoustics Conference, 2005.

[16] C. Canuto, M.Y Hussaini, A.Quarteroni, and T.A Zang. *Spectral Methods in Fluid Dynamics*. Springer-Verlag, Berlin, 1988.

[17] K. Schwartzschild. *Die Beugung und Polarisation des Lichts durch einenSpalt*. i. Mathematische Annalen, 55:177-247, 1902.

[18] G. M. Corcos. *The Structure of Turbulent Pressure Field in Boundary-Layer Flows*. J. Fluid Mech., 18(3):353-378, 1964.

[19] S. E. Wright. *The acoustic spectrum of axial flow machines*. J. Sound Vib. 45, 165-223, 1976.